RESEARCH ARTICLE

Reference Raman spectrum and mapping of *Cryptosporidium parvum* oocysts

Dmitry Malyshev[1] ● | Tobias Dahlberg[1] | Rasmus Öberg[1] ● |
Lars Landström[2] ● | Magnus Andersson[1,3] ●

[1]Department of Physics, Umeå University, Umeå, Sweden

[2]Swedish Defence Research Agency (FOI), Umeå, Sweden

[3]Umeå Centre for Microbial Research (UCMR), Umeå, Sweden

Correspondence
Magnus Andersson, Department of Physics, Umeå University, Umeå 90187, Sweden.
Email: magnus.andersson@umu.se

Funding information
Swedish Department of Defence, Grant/Award Number: A74028; Kempestiftelserna, Grant/Award Number: JCK-1916.2; Umeå University Industrial Doctoral School; Swedish Research Council, Grant/Award Number: 2019-04016; National Microscopy Infrastructure, Grant/Award Number: VR-RFI 2016-00968

Abstract

Cryptosporidium parvum is a protozoan parasite and among the most infectious diarrhea-causing pathogens, leading to severe health problems for malnourished children and immunocompromised individuals. Outbreaks are common even in developed countries, originating from water or food contamination and resulting in suffering and large costs for society. Therefore, robust, fast, and highly specific detection strategies of *Cryptosporidium* are needed. Label-free detection techniques such as Raman spectroscopy have been suggested; however, high-resolution reported spectra in the literature are limited. In this work, we report reference Raman spectra at 3 cm^{-1} resolution for viable and inactivated *Cryptosporidium* oocysts of the species *C. parvum*, gathered at a single oocyst level using a laser tweezers Raman spectroscopy system. We furthermore provide tentative Raman peak assignments for the *Cryptosporidium* oocysts, along with Raman mapping of the oocysts' heterogeneous internal structure. Finally, we compare the *C. parvum* Raman spectrum with other common enterotoxigenic pathogens: *Escherichia coli*, *Vibrio cholerae*, *Bacillus cereus*, and *Clostridium difficile*. Our results show a significant difference between *C. parvum* Raman spectra and the other pathogens.

KEYWORDS

cryptosporidium, laser tweezers raman spectroscopy, raman mapping

1 | INTRODUCTION

Cryptosporidium is a genus of waterborne pathogenic protozoan parasites that cause a severe gastrointestinal disease called cryptosporidiosis.[1] Both humans and animals can be infected, and of particular note are the species that commonly infect humans, *Cryptosporidium parvum* (*C. parvum*) and *Cryptosporidium hominis* (*C. hominis*).[2] Infection can happen through person-to-person contact, animal-to-person contact, or via ingestion

of contaminated food or water.[3] Cryptosporidiosis is one of the most common waterborne diseases and one of the common causes of death among young children (48 000 cases in 2016).[4] Outbreaks occur globally, resulting in >12 million disability-adjusted life-years[4] with high costs for society.[5,6] One of *Cryptosporidium*'s strengths as a pathogen is its ability to form resilient oocysts, which are 5 μm in diameter spherical particles. See SEM images of *C. parvum* oocysts in Figures 1 and S1. Oocysts are non-motile and can remain infective outside the host for
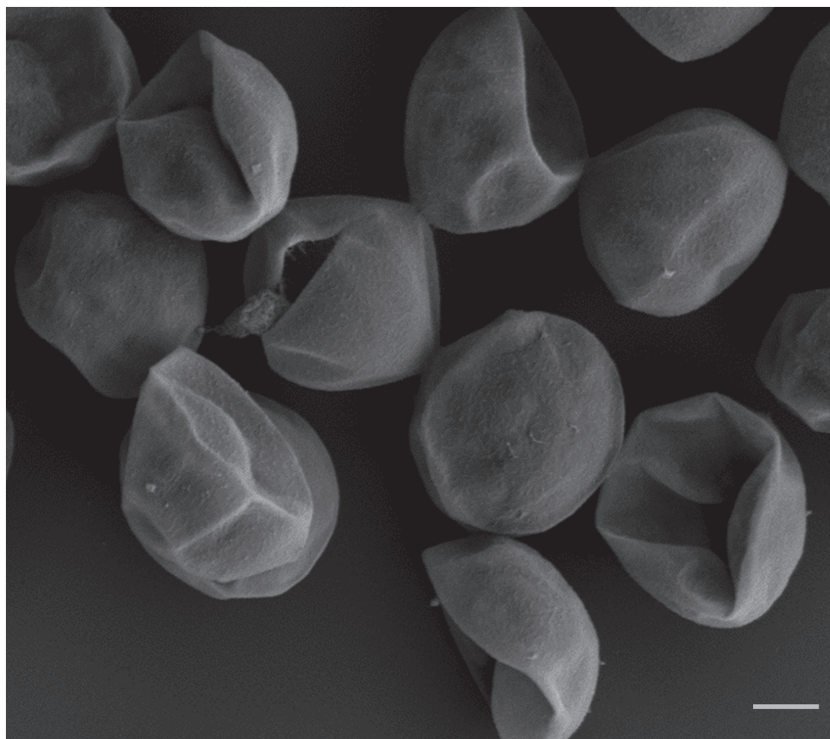
over one year.[7] Each oocyst contains four sporozoites that infect the epithelial cells in the intestine and ingesting as few as 10 oocysts can be sufficient to cause infection in humans.[8,9]

Oocysts can be inactivated with high doses of UV radiation[10]; however, they are highly resistant to chemical decontamination techniques. Ethanol, as well as commonly used chlorine solutions, including bleach, does not kill *Cryptosporidium* oocysts.[7] The suggested protocol for decontaminating water is 5–6% hydrogen peroxide for 20 min.[11,12] Boiling water and drying the oocysts for more than 4 h are also effective decontamination methods, but these methods are not practical in treating larger water sources like water reservoirs or swimming pools.[11] If the decontamination is unsuccessful and a person is infected, the resulting cryptosporidiosis gives similar symptoms as bacterial gastrointestinal pathogens. Bacteria-related diarrhea is often successfully treated using antibiotics; however, *Cryptosporidium* are strongly resistant to most antibiotics since they are not prokaryotes. A misdiagnosis of cryptosporidiosis as a bacterial infection leads to an ineffective antibiotic treatment, which increases mortality and contributes to the evolution of antibiotic-resistant bacteria.[13] Therefore, robust, swift, and highly specific methods to detect *Cryptosporidium* in contaminated water and fecal matter are needed.

Currently, the most widespread technique for detecting *Cryptosporidium* oocysts in water samples is based on fluorescence microscopy in which a sampling step is needed. The oocysts are then separated from the water and other contaminants using specialized filters, after which they are stained with antibody-conjugated fluorescent dyes and detected in a fluorescence microscope. Other conventional methods employ immunological and polymerase chain reaction techniques for detecting oocysts.[14,15] Although there is room for improved efficiency of these methods, for example, by utilizing autofluorescence from the oocysts, these methods in their current form suffer from drawbacks such as being labor-intensive, having high costs, and long detection times.

An alternative label-free and highly specific detection method of biological and chemical content is Raman spectroscopy. Raman scattering approaches provide advantages over other spectroscopic techniques such as IR, since Raman signals are generally not affected by the presence of water and Raman bands are much narrower and thus easier to identify than fluorescence bands.[16,17] Raman spectroscopy, therefore, provides good possibilities for accurate chemical fingerprinting *Cryptosporidium*. Chemical mapping of whole *Cryptosporidium* oocysts based on the average Raman spectrum was performed by Stewart et al.[18] However, Raman peak assignments or the heterogeneity of Raman spectra of different oocysts and the different oocyst components was not part of that study. In addition, normal Raman signals are often significantly weaker than fluorescence signals, which can be problematic for rapid detection as it implies
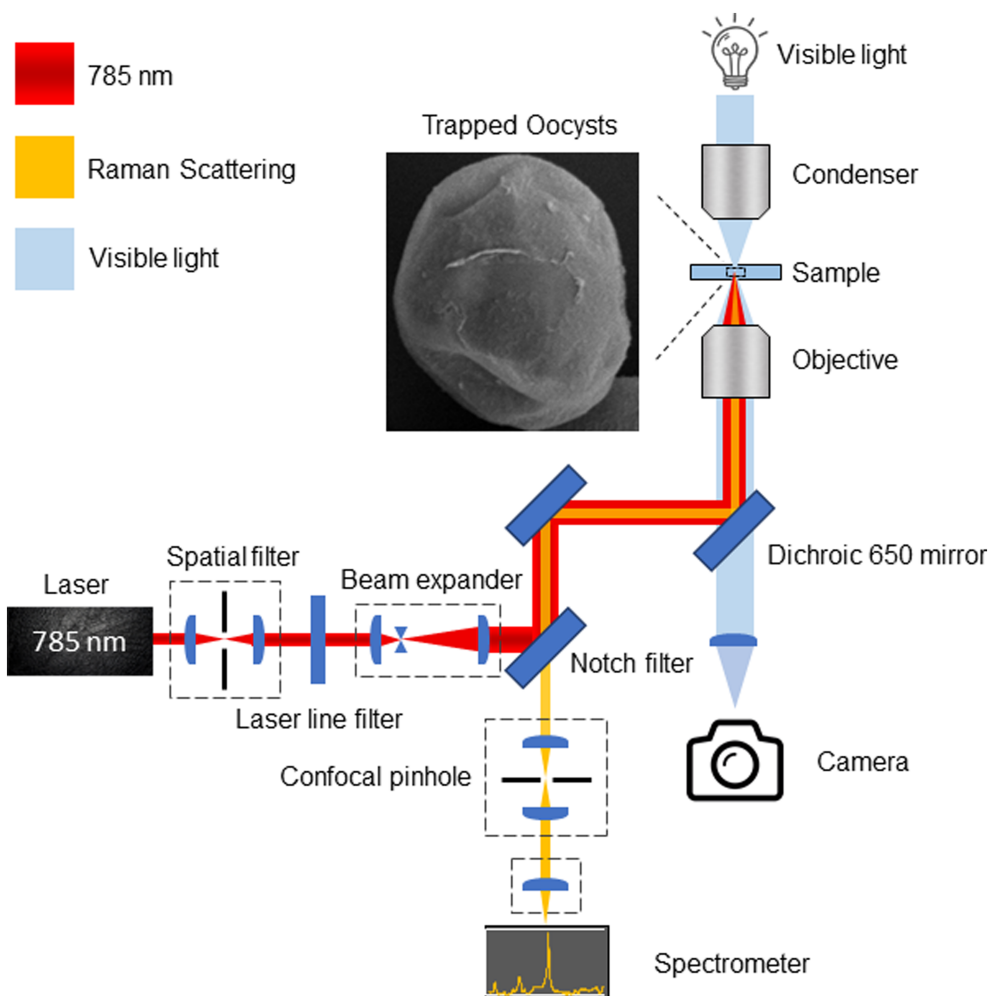
long integration times. To improve Raman signals, surface-enhanced Raman spectroscopy (SERS) has been suggested for *Cryptosporidium* detection.[19,20] However, SERS approaches usually add to the complexity of both system setup and spectral response compared to normal Raman. Furthermore, SERS only gives a strong signal enhancement in close adjacency to the signal enhancing structure. Therefore, only the chemical content of the outer surface is enhanced, making oocysts identification difficult and easily masked by other organic material that can be attached to its surface. Normal Raman is therefore simpler to use; however, to our knowledge, there is currently no high-spectral resolution reference Raman spectrum of *Cryptosporidium* in the literature. Also, there is a lack of a *Cryptosporidium* oocysts Raman map that provides spatial information of the structure. Accurate, high-resolution reference spectra are critical for reducing false alarms in classification/identification algorithms.

In this work, we present Raman spectra of both viable and neutralized *C. parvum* oocysts, captured by a Laser Tweezers Raman Spectroscopy instrument (LTRS). We also perform Raman mapping to illustrate the spatial

distribution of individual components in the oocyst. Finally, we compare the Raman spectral signature with those of other common gastrointestinal pathogens to assess the possibilities to discriminate between pathogens.

2 | MATERIALS AND METHODS

2.1 | Experimental setup and measurement procedure

To trap oocysts and acquire Raman spectra, we used our LTRS instrument that is custom-built in an inverted microscope (IX71, Olympus),[21,22] with the schematic of the system shown in Figure 2. We used a Gaussian laser beam operating at 785 nm (Cobolt 08-NLD) that is coupled into the microscope using a dichroic shortpass mirror with a cut-off wavelength of 650 nm (DMSP650, Thorlabs). Imaging and focusing of the beam were achieved by a 60 × water immersion objective (UPlanSApo60xWIR, Olympus) with a numerical

aperture of 1.2 and a working distance of 0.28 mm. The same laser was used for Raman light excitation. In general, we operated the laser at a fixed output power of 100 mW corresponding to a power of about 60 mW in the sample (total energy of 1.2 J when exposed for 20 s).

We collected the backscattered light by the microscope objective and passed it through a notch filter (NF785-33, Thorlabs) to reduce the Rayleigh scattered laser line. Further, to increase the signal-to-noise ratio, we have mounted a 150 μm diameter pinhole in the focal point of the telescope. The filtered light is coupled into our spectrometer (Model 207, McPherson) through a 150 μm wide entrance slit where a 600 grooves/mm holographic grating disperses the light.[23] The Raman spectrum was then captured using a Peltier cooled CCD detector (Newton 920N-BR-DDXW-RECR, Andor) operated at $-95°$C. Our system has a Raman wavenumber spectral resolution of <3 cm^{-1} and accuracy of $\sim$ 3 cm^{-1}.

2.2 | Strains, culture media, and conditions

We used oocysts of the species *Cryptosporidium parvum* (Iowa isolate), aged 1 to 2 months when measured (Waterborne Inc, New Orleans). The supplied oocysts were harvested from infected calves, extracted from feces with diethyl ether, and purified using percoll density gradient centrifugation. Viable oocysts were stored in PBS, with penicillin, streptomycin, gentamicin, amphotericin B, and 0.01% polysorbate 20. Neutralized oocysts were stored in PBS with 5% Formalin and 0.01% polysorbate 20. Stocks were stored at 4°C. To purify and remove storage solution, oocysts were washed twice by centrifuging at 3000 rcf for 2 min, with sterile water, with the supernatant discarded.

We used *Vibrio cholerae* (*V. cholerae*) str. *El Tor* clinical isolates N16961.[24] These bacteria were provided by Felipe Cava (Umeå university). We grew bacteria using standard laboratory conditions. Cultures were streaked onto LB plates with 200 μg ml^{-1} streptomycin, and single colonies were selected and grown overnight in TG Broth (5 g L^{-1} Tryptone, 10 L^{-1} NaCl, 5% glycerol) at 30°C and sub-cultured in fresh TG Broth before measurement.

We grew *Escherichia coli* (*E. coli*) HB101/pHMG93 cells using LA plates supplemented with 100 μg ml^{-1} kanamycin at 37°C for 24 h.[25]

Clostridium difficile (*C. difficile*) DS1813 spores were provided by Les Baillie (Cardiff University). Spores were grown on BHIS agar at 37°C for 4 days. The cells were collected, left overnight to sporulate, and then purified using density gradient centrifugation in 50% sucrose as described previously.[26] Spores were then washed in deionized water and stored at 4°C.

Wild type *Bacillus cereus* (*B. cereus*) strain NVH 0075-95 spores were provided by Marina Aspholm (Norwegian University of Life Sciences) and stored at 4°C. For the preparation of these, see Pradhan et al.[27]

2.3 | Sample preparation and reference spectrum acquisition

We prepared a sample by placing a 1 cm diameter ring of 1 mm thick vacuum grease on a 24 mm × 60 mm glass coverslip. We added 5 μl of the oocyst suspension into the ring, after which we sealed it by placing a 23 mm × 23 mm glass coverslip on top. After the sample was placed in the LTRS instrument, we measured the Raman spectra using two accumulations of 10 s for spores and oocysts and using two accumulation of 90 s for bacterial cells. We measured on 100 individual oocysts each for both viable and neutralized oocysts and averaged the spectra.

## 2.4 | Data processing and analysis for reference spectra

We used an open-source Matlab script provided by the Vibrational Spectroscopy Core Facility at Umeå University to process Raman spectra.[28] To baseline correct the spectra, we used an asymmetrical least-squares algorithm[29] with $\lambda = 10^4$ and $p = 10^{-3}$. We smoothed spectra using a Savitzky-Golay filter[30] of polynomial order 1 and a frame rate of 5. Graphs were plotted in Origin 2018 (OriginLab).

Principal component analysis was carried out in Graphpad Prism 9.

2.5 | Raman mapping

To perform Raman mapping, we placed 5 μl of the oocyst suspension in water between two 0.25 mm thick quartz coverslips (Alfa Aesar), separated by a 1 mm PDMS ring. We then find a settled oocyst and take sequential measurements of the Raman spectrum starting from the top left and moving in 1 μm steps using the piezo stage (PI-P5613CD, Physik Instruments), for a final mapping area of 5 μm by 4 μm (30 pixels per oocyst). We performed two accumulations at each location to cover the same spectral range of 600–1780 cm^{-1} as in other measurements. We measured on five individual oocysts.

FIGURE 3 Raman spectrum of viable (black) and neutralized (red) *C. parvum* oocysts. Each spectrum is an average of spectra from 100 individual oocysts and the background has been subtracted [Colour figure can be viewed at wileyonlinelibrary.com]
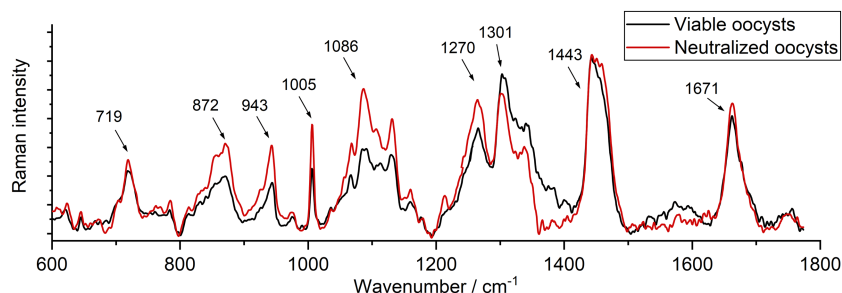
To create Raman maps, we processed spectra into a map using an in-house Matlab script. In the script, we began by background-correcting the spectra in two steps. First, we subtracted a measured background spectrum. Next, we removed any residual background using asymmetric least squares.[29] We then smoothed the corrected spectra using Savitzky-Golay filtering. Intensities of relevant spectral peaks (943, 1005, and 1443 cm^{-1}) provided pixel intensity values which were processed by a 2D linear interpolation of the intensities and their spatial coordinates. Next, we normalized the resulting interpolants between 0 and 1 with respect to their maximum and minimum values. Finally, we plotted the interpolated intensity as a color map on top of a brightfield image of the mapped oocyst.

2.6 | SEM imaging of Oocysts

To perform SEM imaging, we dehydrated the oocysts in a series of graded ethanol solutions, starting with 50% ethanol, and subsequent washes in 70%, 80%, 90%, and 100% ethanol. We then placed a suspension drop on the glass slide and let it dry. We then coated the sample with an ~5 nm layer of platinum using a Quorum Q150T-ES sputter coater. We imaged samples by a Carl Zeiss Merlin FESEM electron microscope using InLens imaging mode at magnifications in the range of 15 000X–50 000X.

3 | RESULTS AND DISCUSSION

3.1 | Raman spectra of viable and neutralized *C. parvum*

Since *C. parvum* oocysts are spherical objects of ~ 5 μm diameter, they are clearly observed in brightfield microscopy. With the LTRS instrument, we can thereby trap a single *C. parvum* oocyst and acquire a Raman spectrum. Oocysts can be trapped and moved in three dimensions using only 2.5 mW of laser power (reducing to approximately 1.5 mW in the sample), indicating that they have

TABLE 1 Peak positions and tentative assignments of selected Raman bands of *C. parvum* oocysts

Peak position (cm $^{-1}$)	Tentative assignment	Reference
719	Phospholipid, Adenine	Pezzotti[35] and Maquelin et al.[40]
872	Tryptophan, Galactosamine	Qiu et al[37] and de Gelder et al.[38]
943	Proline, Valine, Galactosamine	Qiu et al[37] and de Gelder et al.[38]
1005	Phenylalanine	Maquelin et al.[40]
1086	Phospholipid	Pezzotti[35] and Maquelin et al.[40]
1270	Phospholipid: Amide III	Pezzotti[35] and Maquelin et al.[40]
1301	Phospholipid	Pezzotti[35] and Maquelin et al.[40]
1443	Phospholipid	Pezzotti[35] and Maquelin et al.[40]
1671	Phospholipid: Amide I	Pezzotti[35] and Maquelin et al.[40]

a rather high index of refraction for light at 785 nm. However, we used 60 mW of laser power and integrated the collected Raman scattered light for 20 s over Raman wavenumber 600–1780 cm^{-1}. The short integration time at this power did not affect the appearance of an oocyst in the microscope, shown in Figure S2, nor the acquired Raman spectrum, indicating no thermal damage, which is of importance to consider since a high dose might damage the trapped object.[31] In total, we measured $n = 100$ viable and neutralized oocysts, respectively, and averaged their spectra into representative graphs as shown in Figure 3. The spectrum generally resembles that published in previous studies,[18] but the high resolution and larger number of biological replicates of our experimental setup show in more detail that oocyst spectra consist of several distinct Raman peaks.
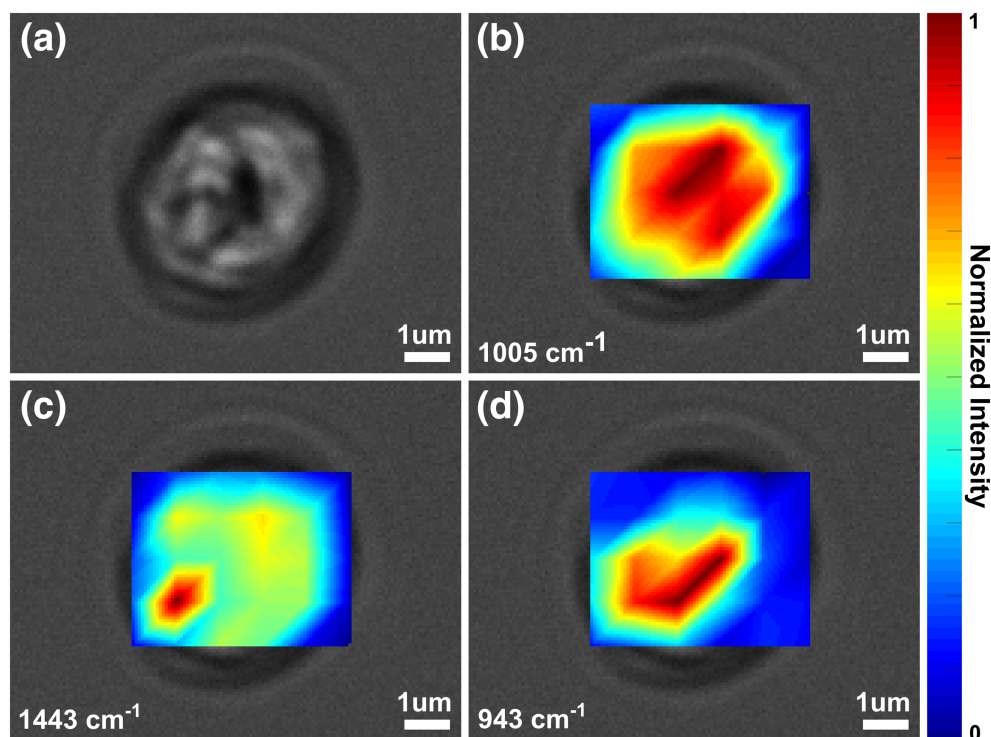
Average Raman spectra of both viable and neutralized oocysts are very similar with no prominent peaks unique to either sample once the background is subtracted; however, a small peak at 1211 cm^{-1} is present among the neutralized oocysts but not the viable ones. Some relative peak intensities are different between neutralized and viable average spectra, with peaks of 867, 943, 1005, 1086, and 1270 cm^{-1} more prominent for neutralized oocysts, while the peak of 1301 cm^{-1} is more prominent for viable oocysts. There is support in published studies that oocysts treated with formalin have their surface chemically altered,[32] and this can explain the difference in Raman spectra. We suggest more studies aimed at assessing the impact of chemicals on oocysts Raman spectra since this is an unexplored field. For example, by trapping oocysts in an LTRS instrument and exposing them to chemicals, one can measure changes and shifts of Raman peaks with time. These experiments can provide relevant information on the chemicals' mode of action on oocysts, similarly to what has been done on bacterial spores.[33] In addition, volume mapping using confocal Raman can provide more details of how sporozoites are organized inside the oocysts.

A tentative assignment of the major peaks is given in Table 1. Raman spectra of the oocysts show peaks associated with amino acids and fatty acids, which is within expectation for the oocysts. In particular, the reported Raman spectra of oleic acid[34] and the related phospholipid phosphatidylcholine show strong similarity to the oocyst spectra. The reported peaks for phosphatidylcholine are at 719, 1088, 1270, 1301, 1442, and 1660 cm^{-1},[35] which closely matches the measured peaks of the oocysts. Phosphatidylcholine was previously reported to be the predominant lipid in the oocysts,[36] which is consistent with our Raman data. Another study failed to find detectable amounts of phosphatidylcholine in the oocyst walls,[32] which indicates that the phospholipid is within the oocyst and not the walls. Two more Raman peaks from the oocyst, situated at 872 and 943 cm^{-1}, are characteristic of several prevalent amino acids such as tryptophan, proline, and valine.[37] They also correspond well to the sharp Raman peaks found from galactosamine.[38] The presence of galactosamine in *Cryptosporidium* oocysts is further mentioned in a study by Stein et al,[39] where the authors suggest that galactosamine is present on the surface of *Cryptosporidium* oocysts, aiding the oocyst in binding to host cells. Finally, the strong 1005 cm^{-1} peak likely corresponds to phenylalanine.[40]

When trapping oocysts and measuring a Raman spectrum, we noted that oocysts were orientated differently in the trap and that peak intensities varied within the population. We hypothesized that different orientations of oocysts and peak variations originated from trapping a non-homogeneous large object, as indicated in Figure 4a. Since oocysts are much larger than the beam waist of the laser used for Raman spectroscopy ($\sim 5 \mu m$ compared to 400 nm beam waist), we only take a spectrum of a small region with a measurement, which can contribute to the variation seen between samples. To resolve this variation,

we Raman mapped oocysts with 1 μm resolution, sampling 30 pixels. A representative Raman mapping measurement of an oocyst illustrating the intensity distribution of three different Raman bands is seen in Figure 4b–d. All five Raman mapped oocysts are shown in Figure S3. The results show heterogeneity in the intensity distribution of the different Raman peaks, which overlaps with structures that are visible in the brightfield image. We speculate that these structures may be the sporozoites, as these would have a different chemical composition than the rest of the oocyst content. The heterogeneity is likely caused by the different viewing angles at which the sporozoites are observed and their location in the oocyst. Since the sporozoites are only 4 × 0.6 μ4m,[41] there are many possible ways they can fit into the oocyst.

We were not able to identify any peaks corresponding to unique oocyst wall components, for example, specific fatty acids, hydrocarbons, and fatty alcohols, as reported by Jenkins et al.[32] However, their concentration may be too low to resolve from other fatty acids, hydrocarbons, and fatty alcohols predominant in the oocysts. Also, the Raman spectra of individual fatty acids have significant overlap,[34] so it is not possible to resolve these as the signal from phosphatidylcholine masks the others.

3.2 | Raman spectra of oocysts are distinct from spectra of other gastrointestinal pathogens

Many microbial pathogens cause acute gastrointestinal disease, the second most common cause of death of children up to 5 years in developing countries.[42] C. parvum belong to this group together with pathogens such as enterotoxigenic E. coli and V. cholerae. In addition, strains of B. cereus and C. difficile are two common food-borne pathogens causing diarrheal disease.[43,44] Identifying the causing pathogen is vital in an outbreak when choosing the right disinfection method and therapeutic approach to diarrheal disease, as well as to minimize the outbreak itself. For Cryptosporidium, this is of particular interest since these infections give similar symptoms as enterotoxigenic E. coli and V. cholerae, which are treated using antibiotics (e.g., tetracycline and fluoroquinolones). However, nitazoxanide is the only FDA approved antiparasitic treatment for Cryptosporidium infections.[45] Thus, it is very important to have a robust detection method that can discriminate between pathogens in order to use the right disinfection approach, and to know what pathogen to treat when a person is infected.

To investigate if it is possible to robustly distinguish the Raman signal from C. parvum with E. coli, V. cholerae, B. cereus, and C. difficile, we also performed single-cell Raman measurements on these pathogens. Representative SEM images of each pathogen are shown in Figures S1 and S4–S7. Since it is known that the cell wall composition and the inner cell of these pathogens are different, we anticipated that the Raman signals should reflect these differences at the single-cell level. For example, as mentioned above, the biochemical composition of the oocyst cell wall structure consists of carbohydrate components, medium and long fatty acids, proteins, and aliphatic hydrocarbons.[32] In comparison, the cell wall of E. coli cells are mainly lipid-rich and contain a peptidoglycan layer further into the cell.[46] For B. cereus and C. difficile, we measured the spectra of spores, the state they are often found in the environment. In spores, the outer layers are protein and peptidoglycan rich, whereas the inner layers consist of up to 25% CaDPA, a common spore biomarker.[47]

In Figure 5, we show Raman spectra of these pathogens alongside the spectrum from C. parvum oocysts. We observe that the Raman spectra of the oocysts differ from those of other non-oocyst pathogens, an observation supported by principal components analysis (PCA) shown in Figures S8 and S9. The spectra form three separate clusters: viable and inactivated oocysts, vegetative cells, and bacterial spores. The projection of the individual components is shown in Figure S10. With regards to differences in the Raman peaks, the most prominent peaks of spore pathogens B. cereus and C. difficile occur at 1017 cm^{-1} in close conjunction with a smaller peak at 1001 cm^{-1}. These two peaks are characteristic peaks of CaDPA. Although these peaks are comparable in appearance to the sharp peak of the Cryptosporidium oocyst appearing at 1005 cm^{-1}, the oocysts are clearly distinguishable from the spore pathogens by their lack of prevalent Raman peaks at 660 and 825 cm^{-1}, as well as their significant activity between 1050 and 1350 cm^{-1}. Comparing the Raman spectrum of the oocysts to those of V. cholerae and E. coli, we similarly observe prominent peaks around 1000 cm^{-1}. Unlike the spore pathogens but similarly to C. parvum, V. cholerae, and E. coli exhibit active Raman spectra with several broad peaks around 1100 and 1250 cm^{-1}. The two can, however, be distinguished from C. parvum by their prevalent peak characteristic of DNA and situated around 780 cm^{-1}, which is largely obscured in the Raman spectrum of C. parvum. The Raman peaks of C. parvum are also significantly more intense in the 1200–1800 cm^{-1}, likely due to the larger amount of phospholipid compared to the cell.
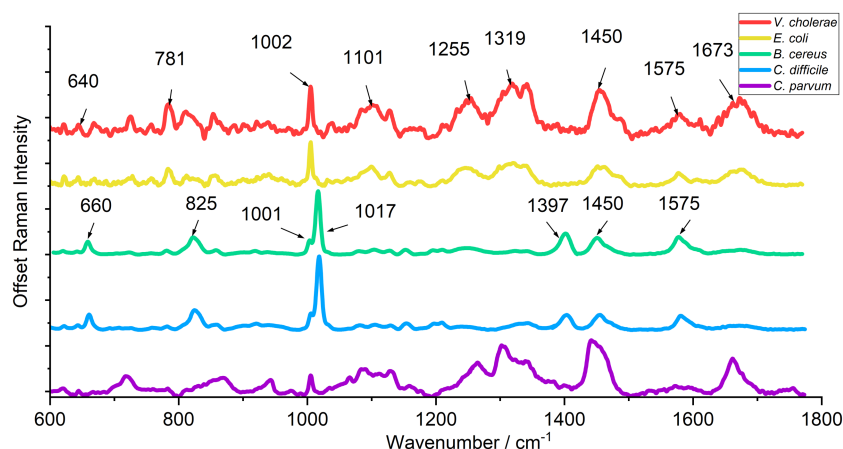
FIGURE 5 Normalized Raman spectra comparison of *V. cholerae* cells (red), *E. coli* cells (yellow), *B. cereus* spores (green), *C. difficile* spores (blue), and *C. parvum* oocysts (purple). The spectra of vegetative cells, oocysts, and spores are clearly distinct from each other, while the spore spectra are very similar. An average of at least 10 samples were used for each spectra [Colour figure can be viewed at wileyonlinelibrary.com]

4 | CONCLUSIONS

Cryptosporidium infections are problematic for humans and animals, resulting in suffering and high costs for society. As symptoms are similar to other enterotoxic pathogens, specific and fast identification of *Cryptosporidium* oocysts is important to use the correct disinfection method and to ordinate the most suitable therapeutic. To assess if normal Raman spectroscopy is suitable to fingerprint oocysts and if their spectra can easily be discriminated from other common enterotoxic pathogens, we measured Raman spectra of single *C. parvum* oocysts using an LTRS instrument. Our results show that spectra of *C. parvum* oocysts are indeed different than those of *V. cholerae* and *E. coli* cells, as well as *B. cereus* and *C. difficile* spores. The Raman signals of viable and formalin neutralized oocysts were, however, largely similar. We also carried out peak assignment of oocysts and identified phosphatidylcholine as one of the major contributors to the Raman spectrum. Our Raman mapping shows that phosphatidylcholine is distributed throughout the oocyst apart from the walls while amino acid-associated peaks are more localized, to a part of any given oocyst, which we believe is the location of the sporozoites. Thus, we conclude that Raman spectroscopy can be used to detect the presence of oocysts in water and that the unique oocysts fingerprint can easily be differentiated from other common gastrointestinal pathogens.

DATA AVAILABILITY STATEMENT
The data that support the findings of this study are available from the corresponding author upon reasonable request.

ORCID
Dmitry Malyshev https://orcid.org/0000-0002-0496-6692
Rasmus Öberg https://orcid.org/0000-0002-0168-0197
Lars Landström https://orcid.org/0000-0001-7370-7777
Magnus Andersson https://orcid.org/0000-0002-9835-3263

REFERENCES
[1] M. W. Riggs, L. E. Perryman, *Infect. Immun.* **1987**, *55*(9), 2081.
[2] M. Bouzid, P. R. Hunter, R. M. Chalmers, K. M. Tyler, *Clin. Microbiol. Rev.* **2013**, *26*(1), 115.
[3] A. Efstratiou, J. E. Ongerth, P. Karanis, *Water Res.* **2017**, *114*, 14.
[4] I. A. Khalil, C. Troeger, P. C. Rao, B. F. Blacker, A. Brown, T. G. Brewer, D. V. Colombara, E. L. De Hostos, C. Engmann, R. L. Guerrant, R. Haque, E. R. Houpt, G. Kang, P. S. Korpe, K. L. Kotloff, A. A. M. Lima, W. A. Petri, J. A. Platts-Mills, D. A. Shoultz, M. H. Forouzanfar, S. I. Hay, R. C. Reiner, A. H. Mokdad, *Lancet Glob. Health* **2018**, *6*(7), e758.
[5] A. Chyzheuskaya, M. Cormican, R. Srivinas, D. O'Donovan, M. Prendergast, C. O'Donoghue, D. Morris, *Emerg. Infect. Dis.* **2017**, *23*(10), 1650.
[6] R. A. Guy, C. A. Yanta, P. K. Muchaal, M. A. Rankin, K. Thivierge, R. Lau, A. K. Boggild, *Parasites Vectors* **2021**, *14*(1), 69.
[7] F. Chen, K. Huang, S. Qin, Y. Zhao, C. Pan, *Vet. Parasitol.* **2007**, *150*(1-2), 13.
[8] W. L. Current, L. S. Garcia, *Clin. Lab. Med.* **1991**, *11*(4), 873.

[9] P. C. Okhuysen, C. L. Chappell, C. R. Sterling, H. L. Dupont, *Clin. Infect. Dis.* **1997**, *25*(2), 428.

[10] F. E. Adeyemo, G. Singh, P. Reddy, F. Bux, T. A. Stenström, *PLoS ONE* **2019**, *14*(5), e0216040.

[11] J. E. Bogan, *J. Dairy Vet. Sci.* **2018**, *7*(4), 1.

[12] S. C. Weir, N. J. Pokorny, R. A. Carreno, J. T. Trevors, H. Lee, *Appl. Environ. Microbiol.* **2002**, *68*(5), 2576.

[13] A. H. Arslan, F. U. Ciloglu, U. Yilmaz, E. Simsek, O. Aydin, *Spectrochim. Acta A Mol. Biomol. Spectrosc.* **2022**, *267*, 120475.

[14] E. M. Hassan, B. Örmeci, M. C. DeRosa, B. R. Dixon, S. A. Sattar, A. Iqbal, *Water Sci. Technol.* **2021**, *83*(1), 1.

[15] G. Luka, E. Samiei, S. Dehghani, T. Johnson, H. Najjaran, M. Hoorfar, *Sensors* **2019**, *19*(2), 258.

[16] P. MacCarthy, J. A. Rice, *Humic Subst. Soil Sediment Water. Geochem. Isolation Charact.* **1985**, April, 527.

[17] D. Wei, S. Chen, Q. Liu, *Appl. Spectrosc. Rev.* **2015**, *50*(5), 387.

[18] S. Stewart, L. McClelland, J. Maier, *Adv. Biomed. Clin. Diagn. Syst. III* **2005**, *5692*, 341.

[19] G. Luka, E. Samiei, N. Tasnim, A. Dalili, H. Najjaran, M. Hoorfar, *J. Hazard Mater.* **2022**, *421*(February 2021), 126714.

[20] K. Rule, P. J. Vikesland, *Environ. Sci. Technol.* **2009**, *43*(4), 1147.

[21] T. Dahlberg, D. Malyshev, P. O. Andersson, M. Andersson, *in Chemical, biological, radiological, nuclear, and explosives (CBRNE) sensing XXI*, (Eds: J. A. Guicheteau, C. R. Howle), SPIE **2020**, 28.

[22] T. Stangner, T. Dahlberg, P. Svenmarker, J. Zakrisson, K. Wiklund, L. B. Oddershede, M. Andersson, *Opt. Lett.* **2018**, *43*(9), 1990.

[23] T. Dahlberg, M. Andersson, *Appl. Opt.* **2021**, *60*(16), 4519.

[24] J. F. Heidelberg, J. A. Elsen, W. C. Nelson, R. A. Clayton, M. L. Gwinn, R. J. Dodson, D. H. Haft, E. K. Hickey, J. D. Peterson, L. Umayam, S. R. Gill, K. E. Nelson, T. D. Read, H. Tettelin, D. Richardson, M. D. Ermolaeva, J. Vamathevan, S. Bass, Q. Halving, I. Dragol, P. Sellers, L. McDonald, T. Utterback, R. D. Fleishmann, W. C. Nierman, O. White, S. L. Saizberg, H. O. Smith, R. R. Colwell, J. J. Mekalanos, C. J. Venter, C. M. Fraser, J. A. Eisen, W. C. Nelson, R. A. Clayton, M. L. Gwinn, R. J. Dodson, D. H. Haft, E. K. Hickey, J. D. Peterson, L. Umayam, S. R. Gill, K. E. Nelson, T. D. Read, H. Tettelin, D. Richardson, M. D. Ermolaeva, J. Vamathevan, S. Bass, H. Qin, I. Dragoi, P. Sellers, L. McDonald, T. Utterback, R. D. Fleishmann, W. C. Nierman, O. White, S. L. Salzberg, H. O. Smith, R. R. Colwell, J. J. Mekalanos, J. C. Venter, C. M. Fraser, *Nature* **2000**, *406*(6795), 477.

[25] M. Goransson, K. Forsman, B. E. Uhlin, *Gene Dev.* **1989**, *3*(1), 123.

[26] D. Malyshev, C. F. Williams, J. Lees, L. Baillie, A. Porch, *J. Appl. Phys.* **2019**, *125*(12).

[27] B. Pradhan, J. Liedtke, M. Sleutel, T. Lindbäck, E. D. Zegeye, K. O'Sullivan, A. K. Llarena, O. Brynildsrud, M. Aspholm, H. Remaut, *The EMBO J.* **2021**, *40*, e106887.

[28] Vibrational spectroscopy core facility. https://www.umu.se/en/research/infrastructure/visp/downloads/accessed22-01-27

[29] P. H. C. Eilers, *Anal. Chem.* **2004**, *76*(2), 404.

[30] M. J. E. Savitzky, A G, *Anal. Chem* **1964**, *36*(8), 1627.

[31] D. Malyshev, R. Öberg, T. Dahlberg, K. Wiklund, L. Landström, P. O. Andersson, M. Andersson, *Spectrochim. Acta A Mol. Biomol. Spectrosc.* **2022**, *265*, 120381.

[32] M. B. Jenkins, B. S. Eaglesham, L. C. Anthony, S. C. Kachlany, D. D. Bowman, W. C. Ghiorse, *Appl. Environ. Microbiol.* **2010**, *76*(6), 1926.

[33] D. Malyshev, T. Dahlberg, K. Wiklund, P. O. Andersson, S. Henriksson, M. Andersson, *Anal. Chem.* **2021**, *93*(6), 3146.

[34] E. Matuszyk, E. Sierka, M. Rodewald, H. Bae, T. Meyer, E. Kus, S. Chlopicki, M. Schmitt, J. Popp, M. Baranska, *Biochim. Biophys. Acta Mol. basis Dis.* **2020**, *1866*(6), 165763.

[35] G. Pezzotti, *J. Raman Spectrosc.* **2021**, *52*(12), 2348.

[36] R. R. Mitschler, R. Welti, S. J. Upton, *J. Eukaryot. Microbiol.* **1994**, *41*(1), 8.

[37] S. Qiu, M. Li, J. Liu, X. Chen, T. Lin, Y. Xu, Y. Chen, Y. Weng, Y. Pan, S. Feng, X. Lin, L. Zhang, D. Lin, *Biomed. Opt. Express* **2020**, *11*(4), 1819.

[38] J. De Gelder, P. Scheldeman, K. Leus, M. Heyndrickx, P. Vandenabeele, L. Moens, P. De Vos, *Anal. Bioanal. Chem.* **2007**, *389*(7-8), 2143.

[39] B. Stein, L. Stover, A. Gillem, K. Winters, J. H. Lee, C. Chauret, *J. Parasitol.* **2006**, *92*(1), 1.

[40] K. Maquelin, C. Kirschner, L.-P. Choo-Smith, N. van den Braak, H. P. Endtz, D. Naumann, G. J. Puppels, *J. Microbiol. Meth.* **2002**, *51*(3), 255.

[41] G. J. Leitch, Q. He, *J. Biomed. Res.* **2012**, *25*(1), 1.

[42] L. Liu, S. Oza, D. Hogan, Y. Chu, J. Perin, J. Zhu, J. E. Lawn, S. Cousens, C. Mathers, R. E. Black, *Lancet* **2016**, *388*(10063), 3027.

[43] E. Kouhsari, S. Abbasian, M. Sedighi, H. F. Yaseri, S. Nazari, A. Z. Bialvaei, P. Dahim, E. Z. Mirzaei, M. Rahbar, *Rev. Med. Microbiol.* **2018**, *29*(3), 103.

[44] F. Qadri, A.-M. Svennerholm, S. G. Faruque, R. B. Sack, *Clin. Microbiol. Rev.* **2005**, *18*(3), 465.

[45] R. V. Anderson, P. M. Curran, *Drugs* **2007**, *67*(13), 1947.

[46] T. J. Silhavy, D. Kahne, S. Walker, *Cold Spring Harb. Perspect. Biol.* **2010**, *2*(5), a000414.

[47] X. Zhang, M. A. Young, O. Lyandres, R. P. Van Duyne, *J. Am. Chem. Soc* **2005**, *127*(12), 4484.

SUPPORTING INFORMATION

Additional supporting information may be found in the online version of the article at the publisher's website.